# An inverse problem approach to identify the internal force of a mechanosensation process in a cardiac myocyte

Serife Arif [a,*], Kokulan Natkunam [a], Byambajav Buyandelger [b], Choi-Hong Lai [a], Ralph Knöll [b,c]

[a] Department of Mathematical Sciences, University of Greenwich, 30 Park Row, London SE 10 9LS, UK
[b] ICMC (Integrated Cardio Metabolic Centre), Karolinska Institutet, Karonlinska University Hospital in Huddinge (M54), SE 141 86 Stockholm, Sweden
[c] AstraZeneca R & D Mölndal, R & D | Innovative Medicines & Early Development Cardiovascular & Metabolic Disease iMed, Pepparedsleden 1, SE 431 83 Mölndal, Sweden

## ARTICLE INFO

## ABSTRACT

Mechanosensation and mechanotransduction are fundamental processes in understanding the link between physical stimuli and biological responses which currently still remain not well understood. The precise molecular mechanism involved in stress and strain detection in cells is unclear. Sarcomeres are the contractile machines of a cardiac myocyte and two main sarcomeric components that are directly involved in the sensation and transmission of mechanical stimuli are titin and filaments (thin and thick). Titin is known as the largest protein in biology with a mass of up to 4.2 MDa. Its flexible region (I-band region) may function as a length sensor ($\varepsilon = l/l_0$) while its Z-disc domain may be involved in the sensation of tension and stress ($\sigma = F/A$). Filaments act as contractile machineries by converting biochemical signals into mechanical work which in response cells either shorten or relax. Based on these considerations and a qualitative understanding of the maladaptation contribution to the development of heart failure, an inverse problem approach is taken to evaluate the contractile force in a mathematical model that describes mechanosensation in normal heart cells. Different functional forms to describe the contractile force are presented and for each of them we study the computational efficiency and accuracy of two numerical techniques.

## 1. Introduction

Cardiovascular disease is the leading global cause of death worldwide with an estimated 17.3 million deaths per year expected to exceed 23.6 million per year by 2030 [1]. The cause of cardiac hypertrophy is known to be from mechanical overloading of cardiac myocytes (induced by, e.g., hypertension or myocardial infarction). There has been at least 230 different mutations identified to cause more than 10 different human diseases [2,3]. A growth factor treatment was used in heart failure patients but was not successful in avoiding the loss of cardiac myocytes. This may indicate the lack of knowledge of the underlying molecular events and thus hindering interference [4]. However, there has been studies that suggest mutations in genes are linked to defects in mechanosensation and mechanotransduction [5]. A comprehensive review on mechanosensation and mechanotransduction in the pathogenesis of heart failure can be found in Linke and Knoll (2010), Knoll and Marston (2012) and Buyandelger et al. (2014) [3–5].

The functional link between cardiac myocyte loss and regeneration as well as the influence of mechanical forces on these events still remain poorly understood [6]. Regeneration and loss are associated with cardiac hypertrophy and its reverse, cardiac atrophy, where there is an increase or decrease in cell size, respectively. This poses a tremendous challenge for every cell since it requires new sarcomeres to be added or removed (growth in 3 dimensions) and membrane constituents to increase or decrease (growth in 2 dimensions) which also cause an increase or decrease in physical stress, respectively. This leads to significant remodelling processes including changes in angiogenesis and the composition of the extracellular matrix [7]. Considering these changes, membrane and cellular components have to change proportionately to find a new equilibrium only within possible limits [8,9].

The development of heart failure can lead to a loss of contractile performance (i.e. the cell's ability to contract and relax). This results in a significant difference in contractile force between normal and heart failure cells. Cellular models that are able to generate realistic contraction patterns in heart cells will be very helpful in understanding diseased-induced alterations in contractile properties. These models contribute to the understanding of cardiac cell contractility in both physiological and pathological contexts at single cardiac myocyte level and may lay the foundation for quantitatively understanding the mechanism of heart failure.

---

In this paper, one aim is to make use of a previously published model that could be used to measure the contractile force in a single cell and propose an inverse problem approach to evaluate the contractile force. This approach could become a useful tool in studying disease-induced alterations in contractile properties at single cardiac myocyte level. The model has been derived based on physical laws and linear elastic theory linking to the sarcomere dynamics (Sections 2 and 3). A brief biological background of the sarcomere dynamics with linkages to the role of intracellular $Ca^{2+}$ dynamics in triggering the contractile mechanism is reviewed (in Section 2) with emphasis on the three important processes and features that contribute to active, passive and viscous forces in muscle contraction: calcium-induced calcium release (CICR), sliding filament theory and the giant molecule titin. The other aim is to provide the origins of the model and encourage future developments. In Section 4, two numerical techniques (i.e. Quantum-behaved Particle Swarm Optimisation (QPSO) and Gauss-Newton (GN)) are used to identify the contractile force and cases are presented in which different functional forms for the contractile force are used. Section 5 is a comparison (i.e. comparing computational accuracy and efficiency) of the results obtained for each case study using either QPSO or GN and wherever suitable a hybrid of these two. The suitability of the method and function in each case are discussed with some possible further improvements in Section 6.

## 2. Excitation-contraction mechanism in normal heart cells

A single muscle cell consists of sarcomeres, each of which extends from one Z-line to the neighbouring Z-line and contains many parallel thin and thick filaments as illustrated schematically in Fig. 1. Thin filaments consist of actin, tropomyosin and C-, I- and T-troponins [10] (two of which are shown in Fig. 1). Thick filaments are mainly composed of myosin and myosin binding proteins [10] (Fig. 1).

The excitation-contraction mechanisms in the cardiac muscle are coordinated by an autonomous electrical activation generated in the sino-atrial node and propagated through the heart wall [11,12]. The membrane goes through depolarisation which causes the opening of voltage-gated channels on the sarcolemma for the influx of $Ca^{2+}$ into the cell triggering a release of $Ca^{2+}$ from the sarcoplasmic reticulum (SR) into the surrounding sarcoplasm [13]. This phenomenon is known as CICR.

The release of $Ca^{2+}$ from the SR binds to TnC sites (Fig. 1) which causes a conformational change in tropomyosin and releases the inhibitory subunit TnI. The troponin/tropomyosin complex shifts to the centre of the groove between actin monomers allowing actin-myosin interaction [14–16]. Myosin heads form crossbridges with
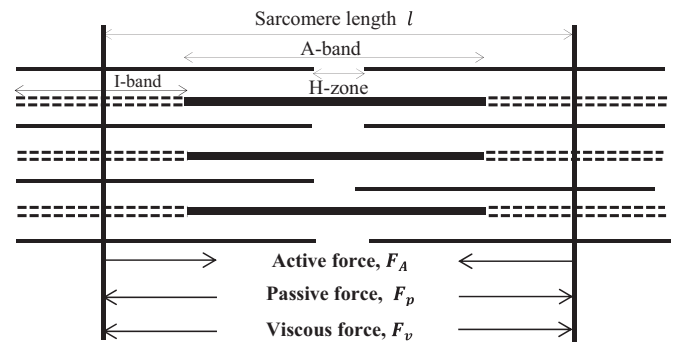
**Fig. 2.** Mechanical model of the sarcomere with directions of active force, $F_A$, passive force, $F_P$, and viscous force, $F_v$, during shortening.

actin by attaching to these active site and perform power strokes by pulling the actin filaments towards the centre of the sarcomere [17]. A series of power strokes causes these filaments to slide along each other (giving rise to the sliding filament theory) thus shortening the muscle [17]. This is the mechanism that is known to cause muscle contraction. However, uncertainties remain associated with the termination of the release of the CICR mechanism which is important for diastolic refilling of the heart [18,19]. $Ca^{2+}$ that is released from the SR appears as $Ca^{2+}$ sparks which propagate as waves throughout the cardiac myocytes. The effects of this in full width cardiac myocyte has recently been experimentally and theoretically investigated [20]. Here a stochastic model for calcium concentration has been used to model the stochastic behaviour of calcium release from channels and was compared to the experimental results. This is known to cause perturbations in the cellular mechanical response which is yet to be studied.

Thin filaments extend from the Z-lines through to the I-bands (where it overlaps with the thick filaments) and terminate on either side of the H-zone (Fig. 2). Thick filaments are connected to the Z-lines through the protein titin and are anchored at the M-line located at the centre of the sarcomere (Figs. 1 and 2) [11]. The sliding filament theory was originally proposed by two papers published consecutively: first by Huxley and Niedergerke (1954), and the other by Huxley and Hanson (1954). They believed that the observed changes in the cross striations of muscle during contraction implied that the actin and myosin filaments are arranged in parallel in the A-band and in the absence of ATP there would be crossbridges formed between them during muscle contraction. In both contraction and stretching, the A-band region remained relatively constant in length until the sarcomere reached the length of the A-band where beyond this point further shortening would fold up the ends of the myosin whereas the I-band
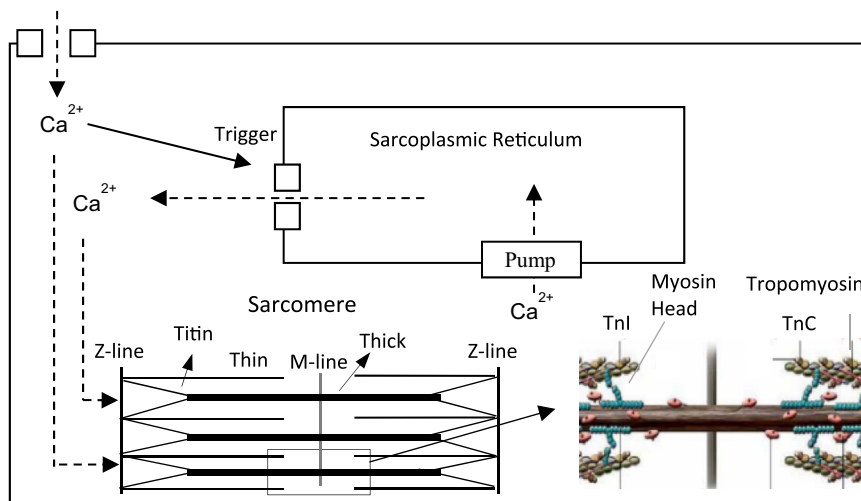
**Fig. 1.** Schematic view of the influx and outflux of calcium in a cardiac myocyte and the CICR process. $Ca^{2+}$ released from the sarcoplasmic reticulum (SR) binds to TnC (leading to contraction) and then $Ca^{2+}$ unbinds from TnC and is pumped back into the SR (during relaxation). Higher magnification around M-line is adapted from [10].

and H-zone of the sarcomere decrease or increase, respectively. The process of stretching would be inhibited by crossbridges between the actin and myosin filaments and the authors refer to evidence that muscles are readily extensible in the absence of these linkages [21,22].

The giant protein titin plays an important part in the sliding of the filaments by maintaining the sarcomeric structural integrity. During stretching and contraction titin is important for thick filaments to remain central in the sarcomere which ensures the development of balanced forces between both halves of the sarcomere [23]. It has a complex structure dependent upon elasticity which contributes to the stress-strain relationship of the cardiac muscle. Each titin molecule spans both the A-band and I-band regions of the sarcomeres (Fig. 2) [24,25]. Titin in the I-band region has been identified as the functionally elastic region that acts like a bidirectional molecular spring responsible for the generation of passive force when stretched or compressed. This region consists of tandemly arranged protein domains which unfold when stretched or compressed and refold when tension is removed. The near Z-disc region of titin is the inextensible region that can withstand compressive forces during shortening. [24].

In the case of no external force, cardiac myocytes are at an equilibrium sarcomere length (slack length) of ~ 1.9 $\mu m$. Titin is highly flexible such that thermally driven bending motions shorten the segment to a near zero end to end length making it appear folded. Stretching the sarcomere increases the end to end length and reduces the bending motions of the extensible region. This gives rise to an opposing force in titin also known as passive force that pulls Z-discs toward each other [24]. In the case of sarcomere shortening below the slack length, titin's extensible region is stretched in an opposite direction of that when elongated and the thick filament moves quite close to titin's near Z-disc region. This generates restoring force pushing the Z-discs away from each other toward sarcomere slack length [24]. These forces generated during sarcomere shortening are demonstrated in Fig. 2. In this paper, the intracellular calcium concentration is not considered thus the model is restricted to the vibration process as described below.

Fig. 2 is a schematic view that represents the contributing forces in sarcomere shortening. The sarcomere compression or stretching is opposed by passive force $F_p$ and viscous damping force $F_v$ (Fig. 2). The passive force $F_p$ is developed by the titin elastic module as described earlier, $F_A$ is a time dependent active force generated by actin-myosin interaction from crossbridge formations. $F_v$ is a viscous damping force which is proportional to the shortening velocity $dl/dt$ where $l$ is the sarcomere length. Therefore, the total force $F_{Total}$ acting upon the sarcomere during contraction can be described as

$$F_{Total} = F_A + F_p + F_v \qquad (1)$$

The sarcomere dynamics is similar to a damped spring-mass system [26,27] and thus the cardiac cell contractile behaviour can be described by a simple vibration model in Eq. (1) [27,28]. Ford, Huxley and Simmons (1976) showed that Stokes's (1851, p. 20) formulation of an oscillating rigid plate in its own plane can be applied to a muscle fiber oscillating parallel to its axis [29,30]. In this paper, a similar formulation is made with constant and numerical values for the cell elastic modulus and viscosity damping factor. The purpose of doing this is to have a mathematical model describing the longitudinal vibration of a cardiac myocyte derived from sarcomere dynamics in order to demonstrate the application of two numerical techniques in such problems to encourage further development. The longitudinal vibration model is described in Section 3.

## 3. Derivation of the vibration model for a single cardiac myocyte

The healthy human myocardium consists of myocytes which are attached to each other to form a spatial network. These cells are usually in cylindrical shape [31] and range in length from 50 to 120 $\mu m$ and in diameter between 5 and 25 $\mu m$. In this paper, a cardiac cell of length 100 $\mu m$ is considered. Cell diameters considered in some models and experiments are: 16 $\mu m$ in the model developed by Courtemanche et al.

(1998) where a mathematical model is developed to describe the action potential of the cell membrane [32] and 27 $\mu m$ in the model developed by Tracqui and Ohayon (2009) where an intracellular calcium model is coupled with a mechanical model [33]. Experimental procedures by Anand et al. (1997) has taken rat left ventricle cardiac myocyte of diameters ranging from approximately 16 $\mu m$ to 23 $\mu m$ [34]. In this paper, a cell with diameter 20 $\mu m$ is considered.

In Eq. (1), the total resultant force $F_{Total}$ acting on a unit sarcomere is proportional to the acceleration of the sarcomere according to Newton's second law of motion, i.e.

$$F_{Total} = ma$$

where $m$ and $a$ are the mass and acceleration of the sarcomere, respectively. Eq. (1) is then rewritten as

$$F_{Total} = F_A(l, t) + F_p(l, t) + F_v\left(\frac{dl}{dt}, t\right) = m\frac{\partial^2 l(t)}{\partial t^2}$$

Assuming the cardiac myocyte has a constant elastic modulus $E$ and cross sectional area, $A$, the passive force (i.e. net elastic force developed by deformation of the titin molecule) may be described by $EA\frac{\partial^2 u(x,t)}{\partial x^2}$ using elastic theory [35] where $u(x, t)$ is the displacement of a unit cell as a function of location and time, and the damping force can be described by $c\frac{\partial u}{\partial t}$ where $c$ is the viscosity damping factor. So the excitation-contraction mechanism in the cardiac myocytes can be described by using the longitudinal vibration model given below

$$\rho A\frac{\partial^2 u(x, t)}{\partial t^2} + c\frac{\partial u}{\partial t} = F_A(x, t) + EA\frac{\partial^2 u(x, t)}{\partial x^2} \qquad (2)$$

where $A$ is a known parameter, $\rho$, the cell density, can be found from published literature and $u(x, t)$ can be obtained by a high-resolution microscope with real-time video output. This model describes the displacement in a single cell during contraction and is previously proposed by Yin et al. (2005). In this paper, the contractile force obtained by Yin et al. [27] based on a moving magnetic bead is adopted. Based on this measurement technique, the external force was generated by applying the magnetic field on a magnetic bead located at the cell end, and the contractile force is derived based on the maximal displacement of cell contraction and magnetic loading force. Both forces are applied in pairs at both ends of the cardiac myocyte with opposite directions. Eq. (2) can then be rewritten into

$$\rho A\frac{\partial^2 u(x, t)}{\partial t^2} + c\frac{\partial u}{\partial t} = EA\frac{\partial^2 u(x, t)}{\partial x^2} + f_{in}(x, t) + f_e(x, t) \qquad (3)$$

where $f_{in}(x, t)$ is the internal force (i.e. contractile force) representing active force due to crossbridge formation and $f_e(x, t)$ is the external loading force representing the magnetic force. In this study, the internal force in Eq. (3) is identified using an inverse problem approach and different functional forms are introduced to study the performance of two numerical techniques.

This section focuses on the derivation of a mathematical model that could be used to measure contractile properties in a single cardiac myocyte. The passive component of cell biomechanical response was derived using linear elastic theory and the active component is left as an unknown term to be determined later using an inverse problem approach. Although this model is proposed previously by Yin et al. (2005), here we derive each of these terms to clarify their linkages to the biophysical phenomenon and establish an understanding of this model for any implementation.

## 4. An inverse problem approach to determine the internal force

For the inverse problem approach, data for displacement and internal force in a single cardiac myocyte is taken from Yin et al. [27]. They propose a measuring technique that involves using a moving magnetic bead to derive the contractile force and mechanical properties of a single cardiac cell. This is done by measuring the contraction force under different levels of magnetic force loading. The measuring system

is mainly based on a high power inverted microscope with video output and edge detection as well as a moving magnetic bead based magnetic force loading module. Initially, maximal displacements of a single cardiac myocyte have been recorded during contraction and then a magnetic bead has been attached on the right end of the myocyte that moves during contraction. Again the contraction processes are recorded under different magnitudes of magnetic force loading by adjusting the field. The formula for the internal force was derived from displacement measured at the right end of the cardiac myocyte under different levels of external forces. The authors showed that the peak displacement values and the magnitude of force load are linearly related. They also showed, through comparison with experimental results, that their proposed method could be used to measure the contractile force of a single cardiac myocyte. This method is proved to be more advantageous over other measuring techniques such as Tarr et al. (1983), Kent et al. (1989), Kawai et al. (1993), Lin et al. (2000), Tan et al. (2002), Laslett et al. (2012) [1,36–40] due to the following: (1) forces can be measured without direct connections to the cell; and (2) the measured force has high sensitivity and a large dynamic range (pN to μN). Due to these advantages, the measurement method in [27] is adopted in an inverse problem approach to evaluate the internal force and the results are used in the validation and optimisation process.
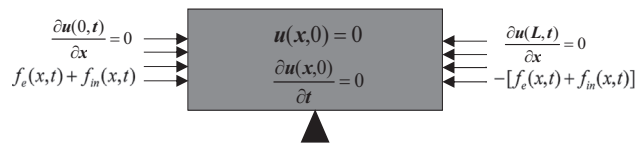
Two numerical techniques, QPSO and GN, are used to identify the internal force (Table 1 Case 5) in Eq. (3) and different functional forms are presented (Table 1 cases 1–4 and 6) in order to study the performance of these techniques. QPSO is a stochastic based method which is a nature inspired algorithm based on swarm intelligence characteristics of birds and fish. Further details on the QPSO and its implementation can be found in [41]. The GN in this study is an iteratively regularised least squares method with a constant damping parameter. This is a gradient based method and thus is very sensitive to initial conditions. An initial approximation close enough can reduce the instability in this method speeding up the convergence of the algorithm. To overcome this sensitivity, the QPSO is used to obtain a good initial approximation for the GN. Here, the computational details are given prior to the application of the inverse problem approach.

The cell centre is fixed at the bottom as illustrated in Fig. 3. This follows from the study by Yin et al. (2005) where the centre of the myocyte is fixed at the bottom in order to prevent intracellular distortion and retain the morphology of myocytes while studying changes in the cellular structure [27].

The initial and boundary conditions from Yin et al. [27] are used. It is assumed that cell fluxes at the boundaries vanish thus the boundary conditions $\frac{\partial u}{\partial x} = 0$ for $x = 0$ and $x = L$ (where $L$ is the length of the cell) are applied at both ends of the cell [27]. These boundary conditions allow cell movement at the ends. The initial conditions used are $u(x,0) = 0$ and $\frac{\partial u(x,0)}{\partial t} = 0$ (Fig. 3). These conditions means that the initial



**Fig. 3.** Representation of the cardiac cell with initial and boundary conditions and force load applied at each end. (Note: this is just a demonstration of how the forces are applied at both ends of the cell and does not represent the computational domain.)

displacement of the cell is zero (i.e. there is no displacement (or movement) in the cell initially). As demonstrated in Fig. 3, the loading force, $f_e(x, t) + f_{in}(x, t)$, is applied at the ends of the cell with opposite directions from time $t = 0.12s$ for approximately 0.65 s. Numerically this is applied everywhere in the cell except for the centre where it is fixed. This is necessary for the convergence of the numerical schemes. The applied external force is given as

$$f_e(t) = \begin{cases} 8.4 \times 10^{-7} & \text{N} \quad x < x_c \\ 0 & \quad x = x_c \\ -8.4 \times 10^{-7} & \text{N} \quad x > x_c \end{cases}$$

where $x_c$ is centre of the cell which is fixed.

Any inverse problem approach involves the evaluation of an objective function, which in this case, can be defined as Least Squares (or the residual sum of squared errors) of the pointwise discrepancies between the model output and the measurement (at the right end point of the cell)

$$J(f_{in}) = \| u(f_{in}; t) - u_{meas}(t) \|_2^2$$

where $u(f_{in};t)$ is the time varying displacement model output with the internal force, $f_{in}$, and $u_{meas}(t)$ is the time varying measured displacement. The aim of this optimisation problem is to determine the internal force, $f_{in}$, which minimises the functional $J(f_{in})$. The displacement model output is obtained by solving the partial differential equation (PDE) in Eq. (3) using the finite difference method (FDM, here, the fully implicit scheme is used as the PDE solver). The implicit scheme is unconditionally stable and convergent ($O(\Delta x^2, \Delta t)$) for this problem.

For the FDM simulations, the computational grid is divided into $N_x$ number of spatial grid points with grid size $\Delta x = x_{i+1} - x_i = \frac{L}{N_x}$ and $N_t$ number of temporal steps with step size $\Delta t = t_{k+1} - t_k = \frac{T}{N_t}$, $k = 0, 1, …, N_t$, (where $T$ is the total simulation time). The spatial and temporal terms in Eq. (3) are discretised using second and first (forward Euler) order centred differences derived from the Taylor series. Using standard finite difference notation the displacement at spatial position $(i+1)$ and temporal position $(k+1)$ is discretised as below:

$$\frac{\partial^2 u}{\partial x^2} = \frac{u_{i+1, k+1} - 2u_{i,k+1} + u_{i-1,k+1}}{\Delta x^2}$$

$$\frac{\partial^2 u}{\partial t^2} = \frac{u_{i, k+1} - 2u_{i,k} + u_{i,k-1}}{\Delta t^2}$$

$$\frac{\partial u}{\partial t} = \frac{u_{i, k+1} - u_{i,k-1}}{2\Delta t}$$

The computational grid given in Fig. 4 demonstrates the FDM using central differences as given above. Grid points in dashed lines are used as ghost points to approximate displacement at the two boundaries.

The computational details with the initial and boundary conditions, and the applied forces are all given and we can now apply the inverse problem approach to Eq. (3) to identify the internal force. In Table 1 Case 5, initial data is generated randomly within a specified interval and is optimised to obtain the internal force in terms of data points. Cases 1–4 and 6 involve different functional forms for the internal force. In cases 1–3, the internal force, $f_{in}(L, t)$, is assumed to be either of the following: a polynomial of order 21 (Case 1), a piecewise polynomial split into two time intervals-one of order 5 in $0.12 \leq t \leq 0.2$ and the other of order 8 in $0.2 < t \leq 0.825$ (Case 2), and

**Table 1**
Functional forms for the internal force profile used in the inverse problem approach and the algorithm used for each case.

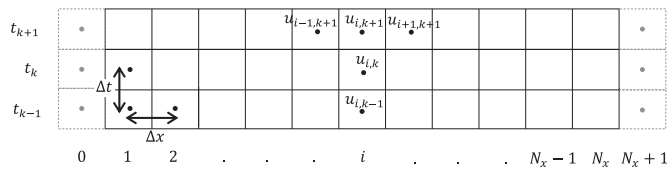| Case | $f_{in}$ (L,t) | Algorithm |
|---|---|---|
| 1: | $f_{in}(L, t) =$ polynomial of order 21, $0.12 \leq t \leq 0.825$ | QPSO and GN |
| 2: | $f_{in}(L, t) = \begin{cases} \text{polynomial of order 5}, 0.12 \leq t \leq 0.2 \\ \text{polynomial of order 8}, 0.2 < t \leq 0.825 \end{cases}$ | QPSO and GN |
| 3: | $f_{in}(L, t) = \begin{cases} \text{polynomial of order 5}, 0.12 \leq t \leq 0.2 \\ \text{polynomial of order 8}, 0.2 < t \leq 0.765 \\ \text{polynomial of order 6}, 0.765 < t \leq 0.825 \end{cases}$ | QPSO and GN |
| 4: | $f_{in}(L, t) =$ Fourier series with 22 terms, $0 \leq t \leq 1$ (scaled from $[-\pi, \pi]$ to $[0,1]$) | GN |
| 5: | $f_{in}(L, t) =$ random initial data, $0 \leq t \leq 1$ | QPSO |
| 6: | $f_{in}(L, t) = K(t)u(L, t)$ where $K(t) = \begin{cases} \text{polynomial of order 7}, 0.12 \leq t \leq 0.2 \\ \text{polynomial of order 22}, 0.2 < t \leq 0.76 \\ \text{polynomial of order 15}, 0.76 < t \leq 0.83 \end{cases}$ | QPSO |

**Fig. 4.** Schematic diagram of the computational grid with grid points represented as dots and displacement for the $(i, k)th$ position shown as $u_{i,k}$.

a piecewise polynomial split into three time intervals - one of order 5 in $0.12 \leq t \leq 0.2$, one of order 8 in $0.2 < t \leq 0.765$ and the third of order 6 in $0.765 < t \leq 0.825$ (Case 3). In case 4, a Fourier series with 22 terms is used. Finally in case 6, it was assumed that the internal force can be described by K(t)u(x, t) where K(t) is a piecewise polynomial specified over three intervals: one of order 7 in $0.12 \leq t \leq 0.2$, one of order 22 in $0.2 < t \leq 0.76$ and the final of order 15 in $0.76 < t \leq 0.83$.

QPSO is very advantageous for two main reasons: (1) when there is no knowledge or information regarding some terms or parameters in the model it's more convenient to specify an interval and the solution can take any value in this interval based on a random generation; and (2) GN is a gradient based method and thus requires good initial approximations for better convergence of the method. This can be obtained using the QPSO algorithm. Due to these advantages, for cases 1–3 a hybrid method (that integrates GN and QPSO) is used. Initially, the QPSO algorithm is performed for 5–10 iterations to obtain a good enough initial approximation (of polynomial parameters) that could be used in the GN algorithm.

In case 4, only GN is used with a fixed initial approximation. It has worked well in this case and no stability issue was observed. This is due to the nature of the functional form involving the summation of a series of $\sin(nx)$ and $\cos(nx)$in the time domain (Note that the initial condition must be very small since the order of magnitude of the internal force is $10^{-6}$). The general Fourier series is applied to $[-\pi, \pi]$ and needs to be scaled to $[0,T]$ for our time domain. This has been done by a simple transformation of $x=\pi t/(0.5T)$ where $T=1$ is the final time step. For Case 5 and 6, QPSO is used with a specified interval for the initial random data (in Case 5) and initial random data for the polynomial parameters (in case 6).

In this section, the problem is set up where all boundary and initial conditions are known as well as the displacement and external force. This is an ill-posed problem since the internal force term is not known and thus it is suitable to use an inverse problem approach to identify this term. The two numerical techniques proposed for this are QPSO and GN. In Case 5, the QPSO is used to obtain the time variation of the internal force in terms of data points whereas in the rest of the cases different functional forms are presented. In some cases, a hybrid method (i.e. QPSO and GN) is used and found to be more advantageous than using only one of the techniques. In these particular cases, the GN would have convergence issues but when this issue is addressed by using a good initial approximation this would make the method more computationally efficient than the QPSO. This hybrid method can be a very powerful technique to overcome the limitations and thus would be more preferable in other such applications.

## 5. Simulation results

The displacement solutions from the FDM was simulated with the parameters given in Table 2. Note that $N_x$ and $N_t$should be chosen so that a stable solution of the system of linear PDEs is guaranteed if using a FDM explicit scheme. The density of the cell was taken from those values used in [42] for rat myocardial tissue regional densities and $E$and $c$are numerical values that guarantee a solution.

Results using each of the cases presented in Table 1 are graphically shown in Fig. 5 and the least squares error calculated in each case is given in Table 3. The main aim of this study is to identify the internal force in Eq. (3) and investigate the performance of the two techniques

(especially when using different functional forms). This is determined by studying their accuracy in fitting and computational efficiency. In cases where QPSO is used, the population size is set to 50 and maximum iterations to 100. For the hybrid scheme, the GN is set to run for a maximum iteration of 1000, $\alpha=0.0001$ (for cases 2 and 3), $\alpha=0.001$ (for case 1) and $\delta=0.001$ (for cases 1–3). In Fig. 5, cases 2 and 3 give similar results and show good agreement with the measured data (blue solid line) from Yin et al. (2005) but case 3 provides a fit with a slightly smaller error but computationally is less efficient by approximately 87 s. This is due to having more parameters to optimise (22 parameters in case 3 and 15 parameters in case 2). Case 1 involves fitting one polynomial (red dashed dotted line) with 22 parameters and computationally takes approximately 15 s longer in comparison with case 3 and also gives a slightly larger error. This is due to the margin of error of trying to fit one polynomial which cannot describe the internal force very well. As seen in Fig. 5 (top) the peak displacement is not well captured.

The Fourier series performed reasonably well and only required 10 iterations to converge but an oscillation can be observed at the start (i.e. $0<t<0.12$) and at the peak around time $t=0.2$ which adds to the overall error. This is due to Gibbs phenomenon and there are ways to avoid (or reduce the effects of) this issue by using the spectrum-splitting technique [43] but this will not be addressed any further in this study.

Case 5 appears to oscillate around the measured data due to the stochastic approach in QPSO. Although this functional form provides good results as seen in Table 3, it is the second most computationally expensive case which is approximately 6 times as long as that of case 2. Case 6 is the most computationally expensive due to using QPSO to optimise for 47 parameters. This functional form was presented to demonstrate that a formulation involving the PDE variable can give a completely different internal force solution in comparison with the rest. This can be useful in some cases when the internal force term depends on $u$ or is an n$^{th}$ partial derivative of $u$.

## 6. Discussion and conclusion

A vibration model based on the active, passive and viscous force developments in sarcomere shortening is described and linked with the physiology of mechanosensation. An inverse problem approach was taken to identify the internal force in this model using QPSO in Case 5. Different functional forms were presented (cases 1–4 and 6) to study the performance of the numerical techniques. Some of the functions provide a good fit to the internal force function whereas some suffer limitations. It was shown that QPSO is very useful when there is no knowledge regarding the shape of the internal force and thus only an approximate interval needs to be specified to successfully obtain the force. This approach is very useful prior to any attempt to functional

**Table 2**

Biophysical and computational parameters used in the simulations.

| Biophysical/ Computational Parameters | Definition | Value | Units |
|---|---|---|---|
| $L$ | Length of cell | $100 \times 10^{-6}$ | m |
| $N_x$ | Number of spatial grid points | 300 | – |
| $T_{max}$ | Final time step | 1 | s |
| $N_t$ | Number of time steps | 500000 | – |
| $E$ | Cell elastic modulus (Youngs modulus) | 4.07 | N/m$^2$ |
| $A(\pi r^2)$ | Cross-sectional area of cell with radius 10μm | $\pi 10 \times 10^{-6}$ | m$^2$ |
| $c$ | Viscosity damping factor | 0.02 | Ns/m |
| $\rho$ | Cell density | 1.053(1053kg/m$^3$) | g/mL |
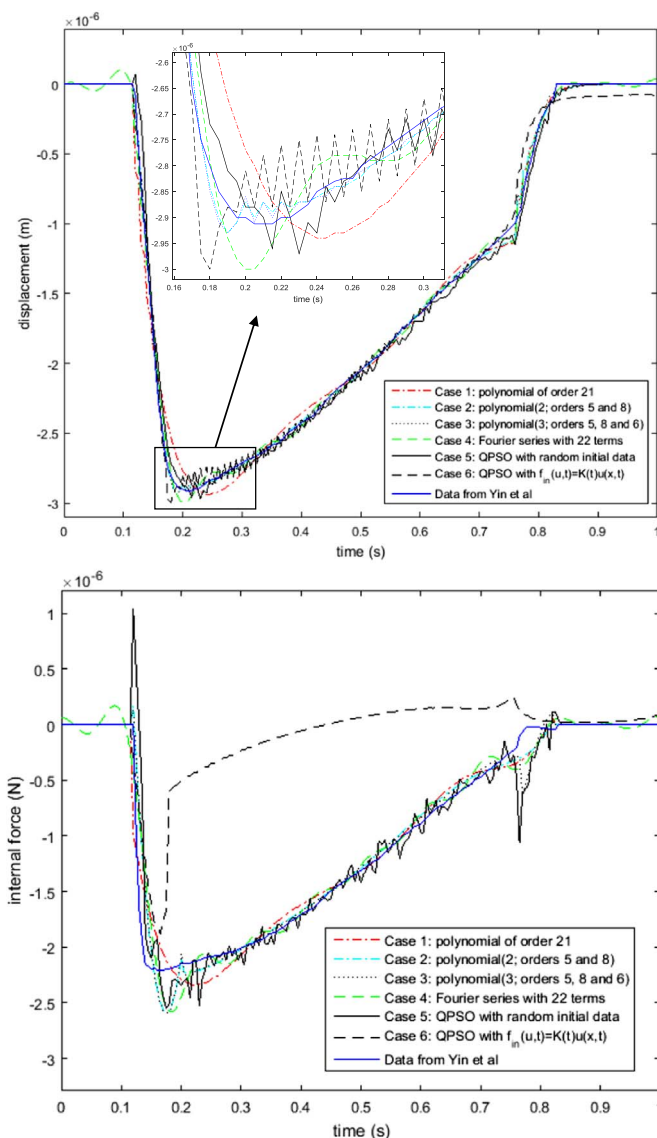
**Fig. 5.** Internal force profiles (bottom) obtained from the numerical techniques using the different functional forms presented in Table 1 and their corresponding displacement outputs (top). Model results for the displacement and internal force are compared with that in [27] (blue solid lines). Internal force outputs are compared with that calculated from the derived formula in Yin et al. (2005) [27].

**Table 3**
Least squares error for data fitting and different functions.

| Case | Functional Form for $f_{in}(t)$ | $L_2$-norm (scaled) | Computational time (s) |
|---|---|---|---|
| 1 | Polynomial in $t$ of order 21 | 1.2557 | 348.4479 |
| 2 | 2 polynomials in $t$ of orders 5 and 8 | 0.4687 | 245.8229 |
| 3 | 3 polynomials $t$ of orders 5, 8 and 6 | 0.3656 | 332.9033 |
| 4 | Fourier series in $t$ with 22 terms | 0.6861 | 3.9060 |
| 5 | QPSO with random initial data | 0.5789 | 1422.1947 |
| 6 | QPSO with $f_{in}(u, K) = K(t)u(x, t)$ | 1.1812 | 1474.0364 |

fitting. From the results in Table 3, we observe an increase in computational time as the number of parameters is increased (Case 5 and 6). This does not seem to be the case for the Fourier series where 23 parameters need to be optimised. This is due to the nature of the function and the margin of error. In the case of the GN, an initial approximation was

obtained from QPSO due to sensitivity to initial conditions. With this study we show that QPSO and GN perform well for evaluating the internal force (i.e. contractile force) in single cardiac myocyte and could be used as a supplementary tool in experimental studies when measuring quantities with biophysical parameters. It is a very useful alternative approach to the measuring technique proposed by Yin et al. (2005). The vibration model considered in this paper can be coupled with an intracellular calcium compartment model which can fully describe the mechanosensation process in a single cell. Inverse problem approach can then be applied to this coupled model to measure contractile force associated with intracellular calcium concentration.

### Acknowledgements

### References

[1] Laslett LJ, Alagona P, Jr., Clark BA, Drozda JP, Jr., Saldivar F, Wilson SR, Poe C, Hart M. The worldwide environment of cardiovascular disease: prevalence,

diagnosis, therapy, and policy issues: a report from the American College of Cardiology. J Am Coll Cardiol 2012;60:S1–49. http://dx.doi.org/10.1016/j.jacc.2012.11.002.

[2] Herrmann H, Bar H, Kreplak L, Strelkov SV, Aebi U. Intermediate filaments: from cell architecture to nanomechanics. Nat Rev Mol Cell Biol 2007;8:562–73. http://dx.doi.org/10.1038/nrm2197.

[3] Buyandelger B, Mansfield C, Knöll R. Mechano-signaling in heart failure. Pflug Arch-Eur J Physiol 2014;466:1093–9. http://dx.doi.org/10.1007/s00424-014-1468-4.

[4] Knöll R, Marston S. On mechanosensation, Acto/myosin interaction, and hypertrophy. Trends Cardiovasc Med 2012;22:17–22.

[5] Linke WA, Knöll RH. Cardiac mechanosensation and clinical implications. Eur J Cardiovasc Med 2010;1:33–7. http://dx.doi.org/10.5083/ejcm.20424884.05.

[6] Mercola M, Ruiz-Lozano P, Schneider MD. Cardiac muscle regeneration: lessons from development. Genes Dev 2011;25:299–309. http://dx.doi.org/10.1101/gad.2018411.

[7] Knöll R, Iaccarino G, Tarone G, Hilfiker-Kleiner D, Bauersachs J, Leite-Moreira AF, Sugden PH, Balligand JL. Towards a re-definition of 'cardiac hypertrophy' through a rational characterization of left ventricular phenotypes: a position paper of the Working Group 'Myocardial Function' of the ESC. Eur J Heart Fail 2011;13:811–9. http://dx.doi.org/10.1093/eurjhf/hfr071.

[8] Sasano T, McDonald AD, Kikuchi K, Donahue JK. Molecular ablation of ventricular tachycardia after myocardial infarction. Nat Med 2006;12:1256–8. http://dx.doi.org/10.1038/nm1503.

[9] Buyandelger B, Mansfield C, Knöll R. Mechano-signaling in heart failure. Pflug Arch Eur J Physiol 2014;466:1093–9. http://dx.doi.org/10.1007/s00424-014-1468-4.

[10] Sarantitis I, Papanastasopoulos P, Manousi M, Baikoussis NG, Apostolakis E. The cytoskeleton of the cardiac muscle cell. Hell J Cardiol 2012;53:367–79.

[11] Keener J, Sneyd J. Mathematical physiology. New York: Springer Science and Business Media, LLC; 1998. http://dx.doi.org/10.1007/978-0-387-75847-3.

[12] Ruiz-Baier R, Gizzi A, Rossi S, Cherubini C, Laadhari A, Filippi S, Quarteroni A. Mathematical modelling of active contraction in isolated cardiomyocytes. Math Med Biol 2014;31:259–83. http://dx.doi.org/10.1093/imammb/dqt009.

[13] Johnson LR. Essential medical physiology, 3rd edition. USA: Elsevier-Academic Press; 2003.

[14] Shiels HA, White E. Commentary: the Frank starling mechanism in vertebrate cardiac myocytes. J Exp Biol 2008;211:2005–13. http://dx.doi.org/10.1242/jeb.003145.

[15] Fearnley CJ, Roderick HL, Bootman MD. Calcium signaling in cardiac myocytes. Cold Spring Harb Perspect Biol 2011;3:a004242. http://dx.doi.org/10.1101/cshperspect.a004242.

[16] Golan DE, Tashjian AH, Armstrong EJ, Armstrong AW. Principles of pharmacology: the pathophysiologic basis of drug therapy, 3rd edition. Philadelphia: Lippincott Williams & Wilkins; 2012.

[17] Copstead L-EC, Banasik JL. Pathophysiology, 5th edition. Elsevier-Saunders; 2013.

[18] Bers DM. Cardiac excitation-contraction coupling. Nature 2002;415:198–205. http://dx.doi.org/10.1038/415198a.

[19] Dupont G, Falcke M, Kirk V, Sneyd J. Models of calcium signalling. Switzerland: Springer International Publishing; 2016.

[20] Chen X, Guo L, Kang J, Huo Y, Wang S, Tan W. Calcium waves initiating from the anomalous subdiffusive calcium sparks. J R Soc Interface 2013;11:20130934. http://dx.doi.org/10.1098/rsif.2013.0934.

[21] Huxley AF, Niedergerke R. Structural changes in muscle during contraction; interference microscopy of living muscle fibres. Nature 1954;173:971–3. http://dx.doi.org/10.1038/173971a0.

[22] Huxley H, Hanson J. Changes in the cross-striations of muscle during contraction and stretch and their structural interpretation. Nature 1954;173:973–6. http://dx.doi.org/10.1038/173973a0.

[23] Tskhovrebova L, Trinick J. Titin: properties and family relationships. Nat Rev 2003;4:679–89. http://dx.doi.org/10.1038/nrm1198.

[24] Granzier HL, Labeit S. The giant protein titin: a major player in myocardial mechanics, signaling and disease. Circ Res 2004;94:284–95. http://dx.doi.org/10.1161/01.res.0000117769.88862.f8.

[25] Luther PK. The vertebrate muscle z-disc: sarcomere anchor for structure and signalling. J Muscle Res Cell Motil 2009;30:171–85. http://dx.doi.org/10.1007/s10974-009-9189-6.

[26] Polyanin AD. Handbook of linear partial differential equations for engineers and scientists. Boca Raton: Chapman & Hall/CRC Press; 2002.

[27] Yin S, Zhang X, Zhan C, Wu J, Xu J, Cheung J. Measuring single cardiac myocyte contractile force via moving a magnetic bead. Biophys J 2005;88:1489–95. http://dx.doi.org/10.1529/biophysj.104.048157.

[28] Yin S, Chen C-L, Cheung JY. Using optical particle image velocimetry for the non-destructive measurement of the single-cell contractile force. Micro Opt Technol Lett 1996;13:31–5. http://dx.doi.org/10.1002/(SICI)1098-2760(199609)13:1 < 31::AID-MOP11 > 3.0.CO;2-8.

[29] Ford LE, Huxley AF, Simmons RM. Tension responses to sudden length change in stimulated frog muscle fibres near slack length. J Physiol 1976;269:441–515.

[30] Stokes GG. On the effect of the internal friction of fluids on the motion of pendulums. Trans Camb Philos Soc 1850;3:1880–905.

[31] Schulte RF, Sachse FB, Werner CD, Dössel O. Rule based Assignment of myocardial sheet orientation. Biomed Tech (Berl) 2000;45:97–102.

[32] Courtemanche M, Ramirez RJ, Nattel S. Ionic mechanisms underlying human atrial action potential properties: insights from a mathematical model. Am J Physiol Heart Circ Physiol 1998;275:H301–H321.

[33] Tracqui P, Ohayon J. An integrated formulation of anisotropic force-calcium relations driving spatio-temporal contractions of cardiac myocytes. Philos Trans A Math Phys Eng Sci 2009;367:4887–905. http://dx.doi.org/10.1098/rsta.2009.0149.

[34] Anand IS, Liu D, Chugh SS, Prahash AJC, Gupta S, John R, Popescu F, Chandrashekhar Y. Isolated myocyte contractile function is normal in postinfarct remodeled rat heart with systolic dysfunction. Circulation 1997;96:3974–84. http://dx.doi.org/10.1161/01.CIR.96.11.3974.

[35] Eslami MR, Hetnarski RB, Ignaczak J, Noda N, Sumi N, Yanigawa Y. Theory of elasticity and thermal stresses: explanations, problems and solutions. Dordrecht: Springer Sci and Business Media; 2013.

[36] Tarr M, Trank JW, Goerts KK. Effect of external force on relaxation kinetics in single frog atrial cardiac cells. Circ Res 1983;52:161–9.

[37] Kent RL, Mann DL, Urabe Y, Hisano R, Hewett KW, Loughnane M, Cooper G. Contractile function of isolated feline cardiocytes in response to viscous loading. Am J Physiol 1989;257:H1717–H1727.

[38] Kawai M, Saeki Y, Zhao Y. Crossbridge scheme and the kinetic constants of elementary steps deduced from chemically skinned papillary and trabecular muscles of the ferret. Circ Res 1993;73:35–50.

[39] Lin G, Pister KSJ, Roos KP. Surface micromachined polysilicon heart cell force transducer. IEEE J MEMS 2000;9:9–17. http://dx.doi.org/10.1109/84.825771.

[40] Tan JL, Tien J, Bhadriraju K, Pirone D, Feel the force: Using a bed of needles to map single cell generated traction forces. In Proceedings of the second joint EMBS-BMES conference, 2: 1648–1649. (doi: 10.1109/iembs.2002.1106582); 2002.

[41] Sun J, Lai C-H, Wu X-J. Particle swarm optimisation: classical and quantum perspectives. CRC Press, Taylor & Francis Group; 2012.

[42] Vinnakota KC, Bassingthwaighte JB. Myocardial density and composition: a basis for calculating intracellular metabolite concentrations. Am J Physiol Heart Circ Physiol 2004;286:H1742–H1749. http://dx.doi.org/10.1152/ajpheart.00478.2003.

[43] Wanguemert-Perez JG, Godoy-Rubio R, Ortega-Monux A, Molina-Fernandez I. Removal of the Gibbs phenomenon and its application to fast-Fourier-transform-based mode solvers. J Opt Soc Am A Opt Image Sci Vis 2007;24:3772–80. http://dx.doi.org/10.1364/JOSAA.24.003772.

**Serife Arif** is currently a PhD student working at the University of Greenwich, Mathematical Sciences Department. She is a member of the Institute of Mathematics and its Applications (IMA). She is very interested in the process of mechanosensation and mechanotransduction in cardiac myocytes. Her current research interests include the mathematical modelling of cardiac myocyte dynamics that will quantitatively contribute to the understanding of these two processes as well as efficient numerical and inverse problem techniques for the simulation of the coupling of electrical activity on the myocyte membrane, intracellular calcium concentration, contraction and relaxation dynamics.

**Kokulan Natkunam** is a researcher at the University of Greenwich in the Mathematical Sciences Department. His main interests include the mathematical modelling in biology and medicine and also the use of numerical and inverse problem methods for biological applications. He currently assists in teaching postgraduate students in Inverse Problem, Complex Systems, CFD and Computational Methods.

**Dr. Byambajav Buyandelger** is currently Assistant Professor at Integrated Cardio Metabolic Centre at the Karolinska Institute (ICMC/KI) in Stockholm, Sweden. She has been interested in understanding how cardiac muscle cells sense mechanic signals and respond to it through known as mechanotransduction process which involves in remodelling of physiological function to development of pathological hypertrophy and heart failure. Her current research focuses on dissecting molecular genetic and epigenetic mechanisms of heart failure reduced ejection fraction (HFrEF) and heart failure preserved ejection fraction (HFpEF) using state of art technologies such as RNA-seq and whole genome BS-seq to profile whole genome transcriptome and methylome in genetically altered animal models as well as in human samples. Her findings will contribute to identify novel therapeutic targets to develop epi-drugs for treating HFrEF and HFpEF.

**Professor Choi-Hong Lai** is the Head of the Numerical and Applied Mathematics Research Unit at the University of Greenwich, Mathematical Sciences Department. He is also the program leader for MSc Applicable Mathematics. Editor-in-chief of the journal in the field of computer mathematics, and algorithms and computational technology. Committee panel member of the Institute of Mathematics and its Applications (IMA), Co-chair of the International Symposium of Distributed Computing and Algorithms for Business, Engineering and Sciences, Secretary of the BCS Distributed and Scalable Computing Specialist Group. His main scientific interests focus on Inverse Problems and Optimisation, Computational Medical Biology, and innovative numerical mathematics.

**Professor Ralph Knöll** is Chief Scientist with AstraZeneca and Principal Investigator at the recently established Integrated Cardio Metabolic Centre at the Karolinska Institute (ICMC/KI) in Stockholm, Sweden. He is based both at AstraZeneca in Molndal and Cardio Metabolic Centre at the Karolinska Institute (ICMC/KI). He has a strong interest in genetics, physiology and pharmacology of the cardiovascular system. His research aim is to combine the strengths of the ICMC Regenerative Cardiology Program to foster innovative science-based strategies, technologies, and therapeutic platforms towards unraveling the epigenetic mechanisms underlying the biology of human cardiac disease. The program will capitalize on the internal strengths of KI in the fields of regenerative/developmental/human stem cell biology in general, unique and well-curated patient registries and human tissue/cell resources. His program takes advantage of the strengths of AstraZeneca in terms of drug development know-how, chemical screening, larger scale biology/bioinformatics/higher throughput capacity, regulatory and toxicology expertise, large animal model systems, and larger scale production. Also, he will take advantage of AZ/MedImmune (recombinant protein/peptide design and production, biological therapeutics know-how) and collaboration with Moderna Therapeutics (synthetic modified mRNA therapeutics for cardiovascular disease in general).